IOP Publishing Journal of Micromechanics and Microengineering
J. Micromech. Microeng. **27** (2017) 065005 (9pp) https://doi.org/10.1088/1361-6439/aa68cb

Fabrication of through-wafer 3D microfluidics in silicon carbide using femtosecond laser

Yinggang Huang[1], Xiudong Wu[1], Hewei Liu[1] and Hongrui Jiang[1,2,3]

[1] Department of Electrical and Computer Engineering, University of Wisconsin—Madison, United States of America
[2] Department of Materials Science and Engineering, University of Wisconsin—Madison, United States of America
[3] Department of Biomedical Engineering, University of Wisconsin—Madison, United States of America

E-mail: hongrui@engr.wisc.edu

Received 7 January 2017, revised 13 March 2017
Accepted for publication 23 March 2017
Published 25 April 2017

Abstract

We demonstrate a prototype through-wafer microfluidic structure in bulk silicon carbide (SiC) fabricated by femtosecond laser micromachining. The effects of laser fluence and scanning speed on the laser-affected zone are also investigated. Furthermore, the wettability of the laser-affected surface for the target liquid, mineral oil, is examined. Microchannels of various cross-sectional shapes are fabricated by the femtosecond laser and their effects on the liquid flow are simulated and compared. This fabrication approach offers a fast and efficient route to implement SiC-based through-wafer micro-structures, which are not able to be realized using other methods such as chemical etching. The flexibility of manufacturing 3D structures based on this fabrication method enables more complex structures as well. Smooth liquid flow in the microchannels of the bulk SiC substrate is presented. The work shown here paves a new way for various applications such as reliable microfluidic systems in a high-temperature, high radioactivity, and corrosive environment, and could be combined with SiC wafer-to-wafer bonding to realize a plethora of novel microelectromechanical (MEMS) structures.

Keywords: femtosecond laser, micromachining, silicon carbide, microfluidics, harsh environment, hard material

(Some figures may appear in colour only in the online journal)

1. Introduction

Microfluidics has witnessed tremendous growth over the last two decades in applications ranging from biochemical analysis and medical research to microelectronics and optics. It has realized numerous devices such as gas chromatography [1], micro-mixers [2–4], micro-valves [5], micropumps [6], etc. Widely used fabrication techniques for 3D microfluidic devices include soft photolithography [7], thermo-forming such as injection molding [8], and etching, i.e. dry etching with plasma [9] and wet etching with chemical solutions [10]. At present, silicon [11], glass [12], and polymers such as polydimethylsiloxane (PDMS) [13] are the most common materials used in microfluidic systems. They are, however, unable to survive or function satisfactorily in a harsh environment with high temperature [14], and intense radiation [15], and/or corrosive substance [16].

Currently, silicon carbide (SiC) is the most established material for device applications in harsh environments as it is hard, temperature tolerant, chemically inert, resistant to high electric field, and biocompatible [17, 18] due to its wide band gap [17]. SiC has been extensively investigated and used in various applications such as MEMS resonators capable of wider operating frequencies than the polysilicon-based ones [19] and pressure sensors [20]. Most of the SiC-based MEMS devices developed are realized by crystalline SiC thin film deposited on other easy-to-etch bulk substrates, particularly silicon substrate [21]. However, it is still immature to

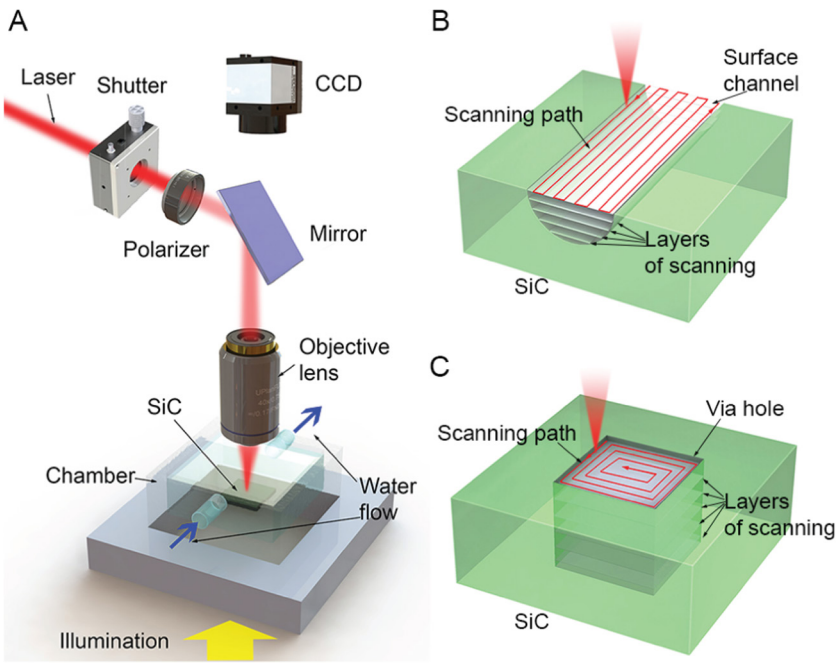

Figure 1. Schematic diagrams of the femtosecond laser micromachining. (A) Optical setup of the laser micromachining system. (B) Laser scanning strategy for the surface channel. (C) Laser scanning strategy for the via hole.

fabricate directly on the bulk SiC substrates that are required for various applications such as all-SiC microsystem devices and through-wafer bonding tailored for a harsh environment. The high thermal stability and chemical inertness make SiC extremely difficult to be etched compared with silicon: for example, potassium hydroxide slightly below 100 °C is widely used to fabricate Si-based devices, whereas the process is not suitable for SiC [22]. Furthermore, both wet- and dry-etching techniques require hard masks such as metal that has high selectivity. However, such masks may contaminate the chambers of plasma etch systems and roughen the surface of a SiC substrate [23], as metal masks, despite being chemically inert, are still etched by the flux of ions in a plasma etching chamber over the long term. Then, micromasking occurs in which the non-volatile by-products generated are redeposited on the sample or in the chamber, thereby reducing the quality of the transferred patterns and gradually degrading the quality of the etch tools. In addition, the etching technique is not applicable for complex 3D device fabrication. The laser direct writing technique has been proposed as an alternative to reactive-ion dry etching due to its simplicity, low-cost, capability of fabricating complex 3D structures, and fast ablation rate for hard materials [24, 25]. Recently, femtosecond laser micromachining has drawn more attention than its longer-pulsed counterparts owing to the advantages of precision micromachining capability, lower thermal and material damage, less sensitivity to target materials, and high repeatability with accurate ablation threshold [26]. Therefore, femtosecond pulsed laser ablation is superior when ablating ultrahard and hard-to-etch materials such as SiC. So far, the femtosecond laser micromachining technique has shown success in ablating SiC films on Si substrates for MEMS devices [27], optical ridge waveguide formation [28], in-air through-hole fabrication in SiC substrates [29], and alcohol-assisted through-hole drilling in SiC [30]. However, the SiC MEMS devices fabricated by femtosecond laser micromachining were restricted to the surface thin film and the SiC through-wafer studies were focused merely on the characterization of the via holes by single shot ablation.

Here, we present a through-wafer fluidic structure consisting of microchannels in bulk 4H–SiC wafer fabricated by deionized water-assisted femtosecond laser micromachining for the first time. It has been reported that the water-assisted near-infrared laser drilling of SiC generates better quality and much less debris than ablating the material in air [31]. High-quality microchannels were achieved with minimal thermal effect around the laser affected zones (LAZs) in which the liquid could flow smoothly. The effects of laser fluence and ablation speed on the dimensions of the trenches that resulted from a single ablation were characterized. In addition, it was found that the surface of the LAZ of SiC is highly attractive to mineral oil with a contact angle of less than 5°. Moreover, the surface morphology of the microchannels comprising the microfluidic structure was characterized by a scanning electron microscope (SEM), while the depth and width of the grooves generated by single ablation were measured by a high-resolution surface profilometer.

2. Experimental details

2.1. Fabrication of microchannels and vias on bulk SiC substrates

The fabrication of microchannels and via holes on the SiC substrates was achieved by a femtosecond laser micromachining system, which is illustrated in figure 1(A). A high-energy fiber femtosecond laser (Uranus2000-1030-1000, Laser-Femto, Inc., USA) with a wavelength of 1030 nm, pulse width of 700 fs, and repetition rate of 121 kHz was transmitted into an objective lens (Mitutoyo, Japan) with a numerical aperture of 0.42

and focused onto the SiC target. The diameter of the focal spot was about 1.5 μm. A mechanical shutter was applied to switch the laser on or off. The power of the laser was adjusted by a polarizer. To achieve a clean surface after the laser ablation, the SiC sample was immersed in a deionized water (DI water) chamber that was mounted on a computer-controlled translation stage (Newport XMS-160, XMS-100, and GTS-30 V for x-, y-, and z-axis, respectively) with the precision of 0.1 μm. The flow rate of the water was about 1 mm s^{-1}. A CCD camera (Thorlabs Inc., USA) was employed for the real-time monitoring of the laser processing. The microchannels and via holes were fabricated by a layer-by-layer ablation process with the laser scanning strategy shown in figures 1(B) and (C), respectively. For the specific structures mentioned in this work, it took approximately 45 min to produce the via hole and 20–40 min to fabricate the microchannels depending on the various cross-sectional shapes.

2.2. Preparation and characterization of the SiC samples

In our experiments, double polished 4H–SiC substrates (N-type doped, CREE, USA) with a thickness of ~350 micrometers were utilized. The wafer was cleaved into $1 \times 1\,cm^2$ square pieces and pre-washed with DI water before the laser ablation. The laser power was measured right before the laser beams hit the DI water surface. After the laser treatment, the samples were cleaned with acetone, methanol, and DI water in an ultrasonic bath for 15 min, respectively. The morphology of the ablated microchannels was characterized by an SEM (Zeiss LEO 1530, Germany) and a high-resolution optical microscope (Nikon Eclipse LV100ND, Japan), while the width and depth of the ablated grooves were measured by a high-resolution surface profilometer (Tencor AlphaStep 200).

2.3. Measurement of contact angle on the SiC surfaces

A goniometer (OCA series, Future Digital Scientific Corp, USA) was used to measure the contact angles of the mineral oil and DI water on the SiC sample surface with and without the laser ablation. The sample was placed on a manually controlled 3-axis stage. The liquid droplet (1.5 μl) was dispensed from a volume controlled pipette onto the sample surface.

To test the wettability of the laser ablated SiC surface, an area of 5x 5 mm^2 on the SiC was ablated by a line-scanning path with a pulse energy of 1.40 μJ and a scanning speed of 1 mm s^{-1}. The laser ablation area was much larger than the dimension of the droplet, so that the contact boundary of the droplet would not touch the edge of the laser-ablated area to ensure the accuracy of the measured contact angle.

2.4. Assembly and characterization of the SiC microfluidic device

To demonstrate the laser micromachining of microfluidics on SiC substrates, a microfluidic device shown in figure 2(A) was fabricated and tested. Two straight microchannels with a diameter of 100 μm and cross-section of a semicircle on both sides of a $1.6 \times 1\,cm^2$ SiC substrate were connected by a via hole, forming a Z-shaped microfluidic channel, as illustrated in figure 2(B). The SiC substrate was flipped to machine the second microchannel, since the laser power was attenuated greatly after traveling through the wafer and thus no ablation could occur. In order to test the flow in the microfluidic system, two pieces of polydimethylsiloxane (PDMS) were pre-treated with oxygen plasma and then bonded on the top and bottom surfaces of the SiC sample, respectively, on a hotplate at 60° for 12 h to facilitate the bonding. The plasma treatment was used to bond the oxidized PDMS surfaces and then seal permanently to create leak-tight microchannels in our microfluidic microchannels. A syringe was used to inject the liquid into the microchannel via a drilled hole in the top PDMS layer. Since the pure fluid could not be observed under the optical microscope, a red solvent-based fluorescent dye (Solvent 250 Red Fluorescent Color Coding Dye, Kingscote Chemicals, USA) was mixed with the liquid to generate a vivid red color to denote the microfluidic path under the optical microscope.

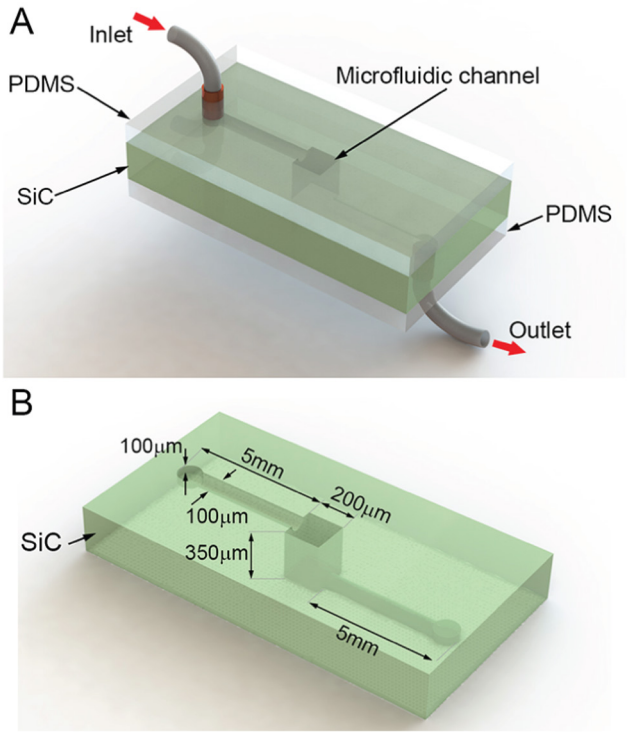

Figure 2. Structural design of the Z-shaped microfluidics on SiC. (A) Schematic diagram of the microfluidic device. (B) Dimensions of the microchannels and via hole on the SiC substrate.

3. Results and discussion

3.1. Influence of laser parameters on ablation rate

Although it has been proved that 1 kHz fs laser pulses could minimize the thermal effects of the ablation process on various metal, dielectric, and semiconductor materials, very few works have provided a systematical study on femtosecond laser ablation on SiC, especially under water-assisted condition. Besides, a higher repetition rate of pulses (121 kHz) in

our experiment would tend to result in thermal accumulation, which would lead to a more remarkable melting-solidification phenomenon of the materials. Therefore, we started our experiment from optimizing the laser pulse energy and scanning speed, the most two important parameters for the laser machining, to improve the ablation morphologies. A series of straight grooves were ablated by single scanning of the laser beam with varying pulse energy and scanning speed.

Figure 3(A) shows the width and depth of the grooves ablated by the laser with different pulse energy ranging from 0.83–4.32 μJ at a translation speed of 1 mm s^{-1}. Both the width and depth of the grooves almost linearly increase as the pulse energy ramps up within the pulse energy range we tested. Meanwhile, the ablation width increases much faster than the ablation depth with respect to the laser fluence increase, since the femtosecond laser has a low thermal penetration depth, i.e. more localization of energy within the depth, whereas more debris generated from higher laser power assisted in more ablation in the surrounding regions. A similar trend was also observed with other translation speeds ranging from 0.1–20 mm s^{-1}. Figure 3(B) shows the width and depth of grooves ablated by the laser with scanning speeds at 0.1, 0.5, 1, 2, 5, 10, and 20 mm s^{-1} with a pulse energy of 2.23 μJ. This indicates that the ablated depth and width decrease with the increase in the scanning speed. During the line scanning process, fewer laser pulses would land on a unit area with a faster scanning speed, which results in a reduced ablation rate. In addition, the decreased rate in the ablation depth is significantly higher than that in the ablation width with increased scanning speed due to the lower thermal penetration depth, as this phenomenon was also found with decreased laser power.

Although high-power laser pulses provide a higher ablation rate, we found that lower laser pulse energy could cause fewer thermal effects as well as much better ablation quality. However, pulse energy lower than 0.83 μJ could not achieve a continuous kerf with measurable width and depth. Therefore, the critical pulse energy for our laser to produce a high-quality groove is considered to be 0.83 μJ, which is the value we used to fabricate microfluidic structures.

In addition, fast scanning can improve the fabrication efficiency but sacrifice the ablation quality, as demonstrated in figure 4. Figure 4(A) shows the SEM image of the feature after one ablation with pulse energy of 4.32 μJ at 20 mm s^{-1}, while figure 4(B) presents one of better quality with the pulse energy of 0.83 μJ at 0.5 mm s^{-1}. No apparent ablation kerf was observed for higher power and scanning speed, whereas a clearly defined ablated path was formed after a single ablation at lower power and speed. Smooth ablation kerf is replaced with a thermally damaged feature if the scanning speed is not carefully calibrated.

3.2. Wettability of the femtosecond laser-ablated surface

The interfacial property of a microfluidic system interacting with the liquids chosen is critical, since it is directly linked to the smoothness, pressure, and velocity distribution of the liquid flow in the microchannels [32]. In the literature, the wetting property of SiC has been studied extensively for liquid

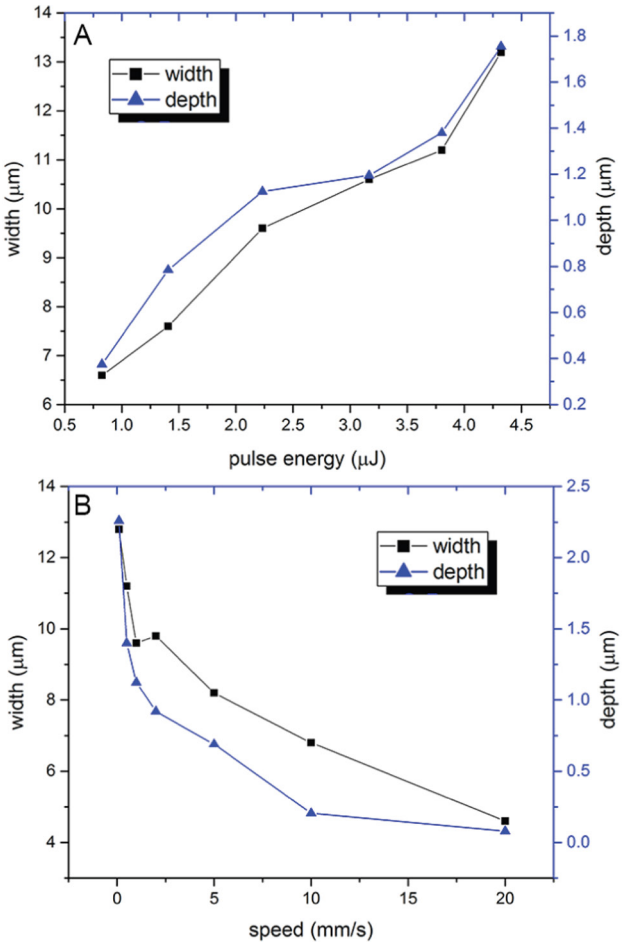

Figure 3. Dependence of the femtosecond laser ablation width and depth on the laser pulse energy (A) and scanning speed (B).

metals [33], binary alloys [34], and even atomic nitrogen [35]. In our study, mineral oil was chosen as the liquid to flow in the microfluidic system for potential harsh environment applications since it has a relatively high boiling point, low thermal and electrical conductivity, and prevents the components of a fluidic system from corroding. The wettability of oil on a SiC surface has not been studied previously. Besides, compared with the lithography-based fabrication methods that produces smooth surfaces of the microchannels, the laser micromachining usually creates special micro- or even nano-structures during the laser-material interactions, which may significantly influence the interfacial properties of the microfluidic devices.

To explore the influence of the surface morphology induced by the laser ablation on the wettability of SiC, we measured the contact angle of mineral oil on the SiC substrate before and after the laser ablation. Figure 5(A) shows the smooth surface of the SiC substrate before laser treatment. The contact angle of the mineral oil is about 21°, indicating a wettable surface of SiC. Figure 5(B) illustrates the surface morphology of the SiC after the laser ablation. The laser-ablated surface shows sub-μm-scale periodic surface roughness compared with the intact surface, and the contact angle of the mineral oil on the laser-ablated SiC surface plummets to a mere 2.9°, which is expected, since the wettability of the surface with the given liquid is improved with increased roughness if the

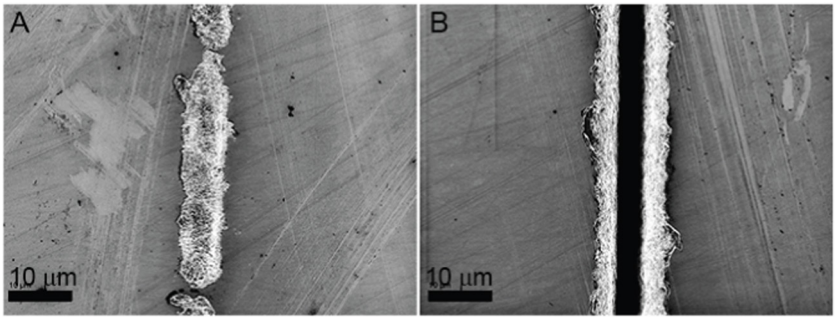

Figure 4. Ablated feature after a single ablation with different pulse energy and scanning speeds. (A) Pulse energy: 4.32 μJ; speed: 20 mm s^{-1}. (B) Pulse energy: 1.4 μJ; speed: 0.5 mm s^{-1}.

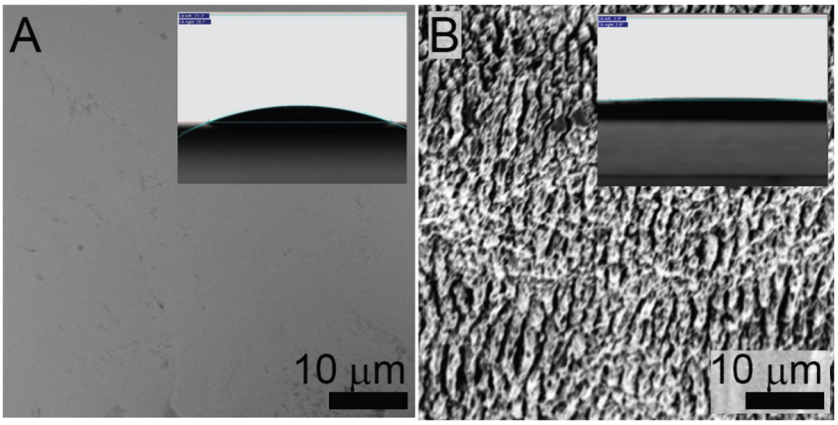

Figure 5. Surface morphology of SiC substrate (A) before and (B) after laser ablation. Inserts in (A) and (B) show the contact angle of mineral oil measured on the SiC surfaces.

surface is wettable with the liquid [36]. The highly wettable characteristics of the oil in the LAZ reduces the pressure needed for it to be injected into and driven through the microfluidic channels. In contrast, the SiC sample surface is not highly hydrophilic for either the clean surface or the LAZ. While the contact angle of water on clean substrate is quite close to 90°, the roughened surface after laser treatment does not greatly increase the hydrophilicity as the contact angle is still close to 85°, indicating that the mineral oil is the more suitable fluid for SiC-based microfluidic systems.

3.3. Control of cross-sectional shape of microchannels

Compared with conventional photo-lithography patterning, which is only able to realize structures with uniform cross-sectional depth from one-time pattern transfer, the femtosecond laser micromachining not only has the advantage of no mask requirement and low cost but its capability of high-precision complex 3D structure manufacturing, including fabricating devices with various cross-sectional shapes. In general, the geometrical design of the cross-section of microchannels in a microfluidic MEMS system has substantial impact on the pressure [37] and flow velocity dynamics [38] of the liquid. Hence, it is indispensable to characterize the microchannels of various cross-sectional shapes during the design process of a microfluidic system.

The fabrication process for microchannels of various shapes was previously investigated. Maselli *et al* reported on a long microchannel with a circular shape on fused silica using femtosecond laser irradiation [39], Welin *et al* demonstrated water flows in trapezoidal silicon microchannels [40], Cheng *et al* varied the cross-sectional shape of microchannels in photostructurable glass [41]. Although microchannels of many regular or irregular shapes have been investigated, the target materials chosen for such studies mostly relied on conventional semiconductors such as silicon, common metals such as nickel and copper, and polymers such as PDMS. Here, we demonstrate microchannels of rectangular, semicircular, and triangular cross-sections in SiC by femtosecond laser micromachining and show the numerical simulations of corresponding cross-sectional velocity flow distributions.

In order to examine the morphology of the ablated surface in the designed structures, top-view SEM images for the three aforementioned microchannels were obtained. Figures 6(A)–(C) show surface images for channels with cross-sectional rectangular, triangular, and semicircular shapes, respectively. All the microchannels are confined by the clear edges and relatively smooth transition inside their trenches. The raised stripes present in the three channels might be attributed to the slight turbulence of the flowing DI water that dispersed laser energy occasionally during the ablation process, which should be addressed in the future.

Figures 6(D)–(F) show the optical images of microchannels of rectangular, semicircular, and triangular shapes, respectively. The samples were processed on a program-controlled stage with a pulse energy of 2.23 μJ and a translation speed of

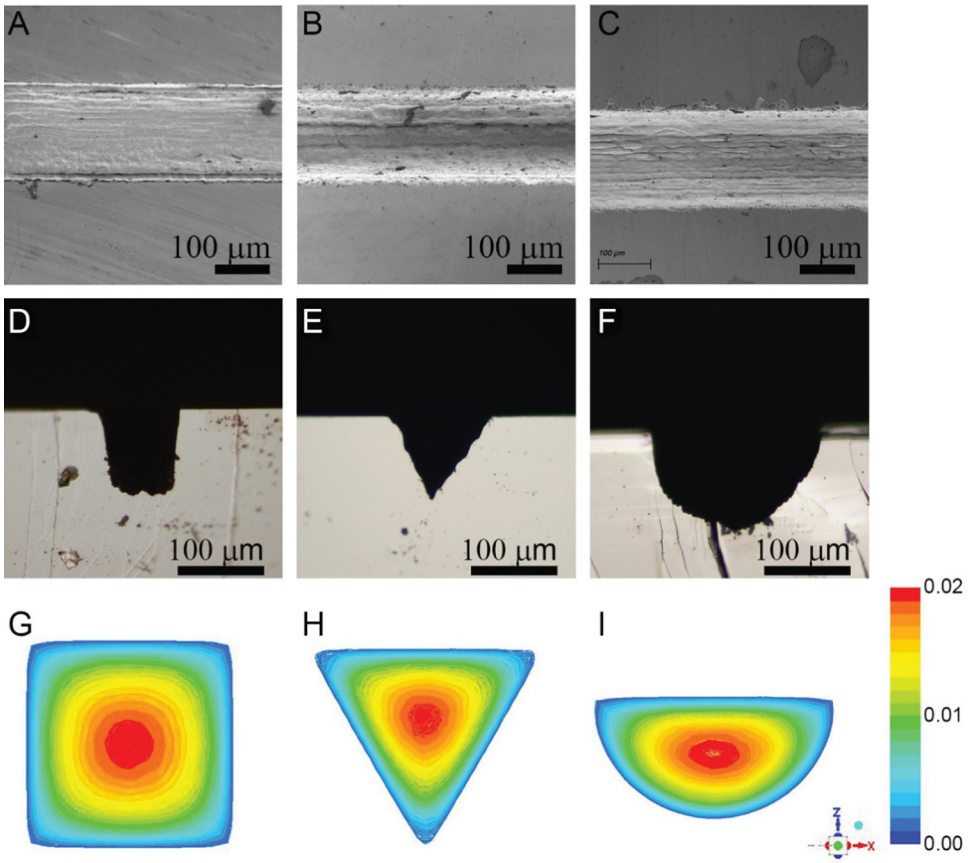

Figure 6. (A)–(C) Surface images of the microchannels with rectangular, triangular, and semicircular shapes, respectively. (D)–(F) Cross-sectional images of the microchannels with rectangular, triangular, and semicircular shapes, respectively. (G)–(I) Steady-state cross-sectional velocity profiles of microchannels with rectangular, triangular, and semicircular shapes, respectively.

5 mm s^{-1} in DI water and with the target 0.1 μm deep. After the ablation process, the samples were rinsed with acetone in an ultrasonic bath for 5 min to remove any remaining debris. The microchannels were processed layer-by-layer with minimal thermal effect and cracking phenomenon.

In an effort to characterize the impact of cross-sectional geometry on the flow properties, Ansys Fluent 17.0 was utilized to simulate the steady-state cross-sectional velocity profile for the mineral oil. Since the Reynolds number is quite low in microscale channels, pressure driven laminar flow mode was selected. Figures 6(G)–(I) illustrate the cross-sectional velocity distribution for rectangular, semicircular, and triangular microchannels, respectively, with the initial velocity of 1 cm s^{-1}. The velocity of the oil near the walls of all three microchannels was set to zero with the assumption of no-slip boundary condition, as required by the basic law of fluid mechanics for pressure-driven laminar flow that produces a parabolic velocity distribution along the flowing direction within microchannels. However, due to the different shapes of the boundary walls, the transverse velocity profile can be squeezed to fit the cross-sectional configurations. Despite the similar trend that the closer the oil is to the center of the geometry, the faster it travels, the area that represents the fastest flowing speed varies for the three microchannels under investigation. The flexibility of creating microchannels of various cross-sectional shapes by femtosecond laser micromachining widens the applications of microfluidics requiring unconventional or non-uniform flowing channels.

3.4. Fabrication of microchannels and via holes on SiC

It is necessary to utilize through-wafer structures when complex 3D microfluidics, such as wafer-to-wafer microfluidics, need to be built. In order to realize a through-wafer microfluidic system, femtosecond pulsed laser was used and the relevant parameters, i.e. translation speed and laser pulse energy, were tuned to obtain the best quality of the surface and through-wafer microchannels. The water film thickness was set slightly over 1 mm, which was found to be the optimal parameter for infrared pulse laser drilling of SiC in the water [31].

Figure 7 illustrates the morphology of the microchannels and the via manufactured by the femtosecond laser micromachining. Figure 7(A) presents the top view of a Y-channel with three legs of identical dimensions with sharp turns at the intersection and minimal thermal damage, indicating the high quality of the ablation by the femtosecond laser. The SEM image of the Y-channel in Figure 7(B) shows the morphology of the laser-ablated microchannel. The overall roughness is in the range of 800 nm–1 μm and the micro- and nano-roughness on the sidewall and bottom of the microchannel could improve the wettability of the microfluidic channel, as demonstrated

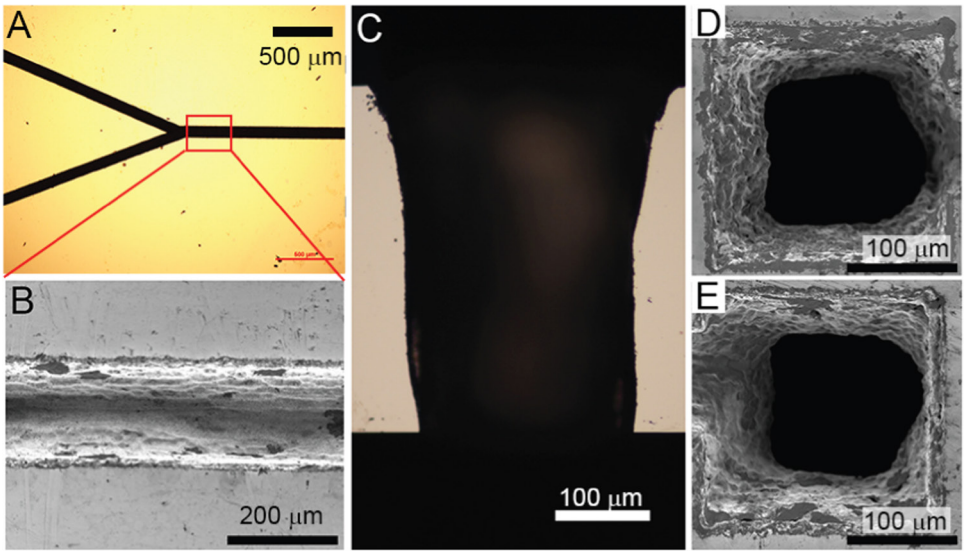

Figure 7. Fabricated surface microchannels and via hole on the SiC substrates. (A) and (B) Optical microscope and SEM images of a Y-shaped microchannel, respectively. (C) Cross-sectional image of the via hole. (D) and (E) Top- and bottom-view SEM images of the via hole, respectively.

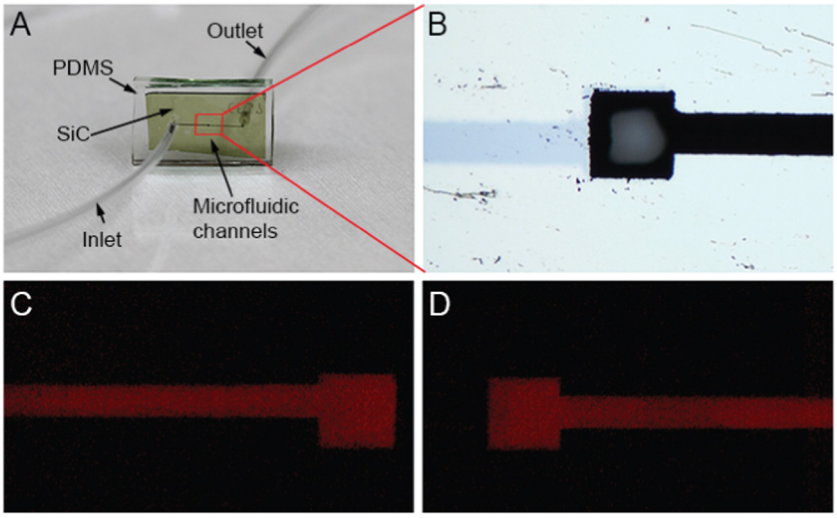

Figure 8. Z-shaped microchannel device demonstrated with mineral oil flowing with red fluorescent dye. (A) Photo of the Z-shaped microchannel device. (B) Image of the microchannels and via hole on the SiC substrate. (C) and (D) Images of the mineral oil flow with red fluorescent dye for bottom and top channels, respectively.

in the section 3.2. The images of the cross-section, top, and bottom view of the via hole are demonstrated in figures 7(C)–(E), respectively. The cross-sectional view indicates a vertical sidewall not readily possible with other manufacturing techniques within a reasonable processing time. The top and bottom views of the via show smooth and clear edges, indicating the minimized thermal damage of the water-assisted femtosecond laser-ablation process. The slightly wider opening of the surface is due to the higher susceptibility of the laser power near the surface region. The top and bottom of the via exhibit the same feature as the cross-section as well as the rough wall, as found in the microchannels on the surface.

3.5. Z-shaped through-wafer microfluidic device

Figures 8(A) and (B) shows a photo of a Z-shaped through-wafer microfluidic device and an image of the microfluidic channel, respectively. The straight microchannels on the top and the bottom of the SiC are 5 mm long, 0.1 mm wide, and 0.1 mm deep, while the width and depth of the via are 0.2 mm and about 0.35 mm, respectively.

Figures 8(C) and (D) demonstrate the oil flow in the top and bottom microchannels, respectively, from the optical microscope. The mineral oil was first mixed with the prepared fluorescent dye, then injected through the hole punched into the PDMS layer and finally the microchannels. Note that the bottom microchannel was displaced from the center of the via slightly to differentiate from the top for convenience of measurement. According to the microscopic image showing the red color filling all areas of the top and bottom microchannels, a smooth liquid flow was achieved throughout the microfluidic channels.

It is interesting to note, however, that the laser power slightly above the ablation threshold did not successfully yield

the best quality microchannel in our experiments. From the previous studies, ablation from lower pulse energies, so long as it is above the threshold, creates cleaner features with less heat-affected zone formation and debris around the patterning areas. This was true in our study only when the ablation took place near the surface. When the ablation continued into the bulk SiC, the defect-activation process occurred, which drastically reduced the ablation threshold fluence [42]. Therefore, the laser power was tuned to a lower value after the ablation continued into the bulk to approximately retain the ablation width and depth for each single scan, which in turn retained the target shape and dimension of the microchannels.

4. Conclusion

In conclusion, a prototype through-wafer microfluidic structure in a bulk 350 μm thick 4H–SiC wafer micromachined by a 1030 nm, 700 fs ultrafast femtosecond pulsed laser ablation system was demonstrated for the first time. A smooth oil flow in the microchannels was achieved, while it was found that the oil is highly attractive to the LAZ area of the SiC substrate. The high-quality microchannels with several different cross-sectional geometries were also realized by the femtosecond laser system and the flowing properties were studied as well. The dimension of the ablated kerf with respect to the speed of the relative motion between the laser focal spot and the sample, and the laser pulse energy was also characterized. This study also indicates that the ultrafast femtosecond pulsed laser is a promising technique for high-precision 3D micromachining with minimal thermal damage for ultrahard materials. The manufactured through-wafer microfluidic system can be used in a harsh environment such as high temperature, corrosive media, high radiation, etc. It also paves the way for the SiC wafer bonding in the packaging of microfluidic MEMS devices to be used in harsh environments.

In the future, we plan to design more complex structures to realize more functionalities based on this system such as microfluidic structures with not only various cross-sectional shapes but curved channels and varied channel dimension along the direction of the fluid flow in the bulk SiC substrate that the conventional photolithography technique cannot accomplish. We also intend to investigate further the micro- and nano-particles generated from the ablation of SiC in the liquid-assisted environment. The critical speed for a given laser pulse energy has not been studied extensively, and has yet to be explored in more depth.

Acknowledgments

The authors gratefully acknowledge Xuan Zhang for the help with data acquisition using the Tencor AlphaStep 200 surface profilometer and Yousuf Al-Moallem for the assistance with contact angle measurements. The research was supported by the College of Engineering, University of Wisconsin—Madison, and H Jiang's Lynn H Matthias and Vilas Distinguished Achievement professorships. This research utilizes the NSF-supported facilities at the University of Wisconsin.

References

[1] Terry S C, Jerman J H and Angell J B 1979 A gas chromatographic air analyzer fabricated on a silicon wafer *IEEE Trans. Electron Devices* **26** 1880–6
[2] Nguyen N T and Wu Z G 2005 Micromixers—a review *J. Micromech. Microeng.* **15** R1–6
[3] Gunther A, Jhunjhunwala M, Thalmann M, Schmidt M A and Jensen K F 2005 Micromixing of miscible liquids in segmented gas-liquid flow *Langmuir* **21** 1547–55
[4] Garstecki P, Fischbach M A and Whitesides G M 2005 Design for mixing using bubbles in branched microfluidic channels *Appl. Phys. Lett.* **86** 244108
[5] Weibel D B, Kruithof M, Potenta S, Sia S K, Lee A and Whitesides G M 2005 Torque-actuated valves for microfluidics *Anal. Chem.* **77** 4726–33
[6] Laser D J and Santiago J G 2004 A review of micropumps *J. Micromech. Microeng.* **14** R35–64
[7] Unger M A, Chou H, Thorsen T, Scherer A and Quake S R 2000 Monolithic Microfabricated valves and pumps by multilayer soft lithography *Science* **288** 113
[8] Attia U M, Marson S and Alcock J R 2009 Micro-injection moulding of polymer microfluidic devices *Microfluid. Nanofluid.* **7** 1
[9] Garra J, Long T, Currie J, Schneider T, White R and Paranjape M 2002 Dry etching of polydimethylsiloxane for microfluidic systems *J. Vac. Sci. Technol.* A **20** 975–82
[10] Grosse A, Grewe M and Fouckhardt H 2001 Deep wet etching of fused silica glass for hollow capillary optical leaky waveguides in microfluidic devices *J. Micromech. Microeng.* **11** 257–62
[11] Van Lintel H, Vandepol F and Bouwstra S 1988 A piezoelectric micropump based on micromachining of silicon *Sensors Actuators* **15** 153–67
[12] Harrison D J, Manz A, Fan Z H, Ludi H and Widmer H M 1992 Capillary electrophoresis and sample injection systems integrated on a planar glass chip *Anal. Chem.* **64** 1926–32
[13] Duffy D C D, McDonald J C J, Schueller O J O and Whitesides G M G 1998 Rapid prototyping of microfluidic systems in poly(dimethylsiloxane) *Anal. Chem.* **70** 4974–84
[14] Young D J, Du J, Zorman C A and Ko W H 2004 High-temperature single-crystal 3C–SiC capacitive pressure sensor *IEEE Sens. J.* **4** 464–70
[15] Srour J R, Marshall C J and Marshall P W 2003 Review of displacement damage effects in silicon devices *IEEE Trans. Nucl. Sci.* **50** 653–70
[16] Fassbender F, Schmitt G, Schöning M J, Lüth H, Buss G and Schultze J-W 2000 Optimization of passivation layers for corrosion protection of silicon-based microelectrode arrays *Sensors Actuators* B **68** 128–33
[17] Casady J B and Johnson R W 1996 Status of silicon carbide (SiC) as a wide-bandgap semiconductor for high-temperature applications: a review *Solid-State Electron.* **39** 1409–22
[18] Mehregany M, Zorman C A, Roy S, Fleischman A J, Wu C-H and Rajan N 2000 Silicon carbide for microelectromechanical systems *Int. Mater. Rev.* **45** 85–108
[19] Nabki F 2009 Silicon carbide micro-electromechanical resonators for highly integrated frequency synthesizers *PhD Thesis* McGill University (http://digitool.library.mcgill.ca/R/NR8CV9GJDCC5ECCQUJ6ES6RLAQ8TJ5Y1VKDKC1QVS1RUSXG47P-03355?func=results-brief)
[20] Jin S, Rajgopal S and Mehregany M 2011 Silicon carbide pressure sensor for high temperature and high pressure applications: influence of substrate material on performance *16th Int. Solid-State Sensors, Actuators and Microsystems Conf.* pp 2026–9

[21] Nishino S, Powell1 J A and Will H A 1983 Production of large-area single-crystal wafers of cubic SiC for semiconductor devices *Appl. Phys. Lett.* **42** 460
[22] Zhuang D and Edgar J H 2005 Wet etching of GaN, AlN, and SiC: a review *Mater. Sci. Eng.* R **48** 1–46
[23] Senesky D G and Pisano A P 2010 Aluminum nitride as a masking material for the plasma etching of silicon carbide structures *IEEE 23rd Int. Conf. on Micro Electro Mechanical Systems (MEMS) (Wanchai, Hong Kong)* pp 352–5
[24] Zhang J, Sugioka K, Wada S, Tashiro H and Toyoda K 1997 Direct photoetching of single crystal SiC by VUV-266 nm multiwavelength laser ablation *Appl. Phys.* A **64** 367–71
[25] Zhang J, Sugioka K, Wada S, Tashiro H, Toyoda K and Midorikawa K 1998 Precise microfabrication of wide band gap semiconductors (SiC and GaN) by VUV–UV multiwavelength laser ablation *Appl. Surf. Sci.* **127–9** 793–9
[26] Chichkov B N, Momma C, Nolte S, von Alvensleben F and Tünnermann A 1996 Femtosecond, picosecond and nanosecond laser ablation of solids *Appl. Phys. A Mater. Sci. Process.* **63** 109–15
[27] Dong Y 2004 Femtosecond pulsed laser ablation and patterning of 3C–SIC films on SI substrates for MEMS fabrication *PhD Thesis* Iowa State University (http://lib.dr.iastate.edu/cgi/viewcontent.cgi?article=2153&context=rtd)
[28] Luan Q, Jia Y, Wang Y, Akhmadaliev S, Zhou S, Vázquez de Aldana J R, Tan Y and Chen F 2014 Optical ridge waveguides in 4H–SiC single crystal produced by combination of carbon ion irradiation and femtosecond laser ablation *Opt. Mater. Express* **4** 1166–71
[29] Khuat V, Ma Y, Si J, Chen T, Chen F and Hou X 2014 Fabrication of through holes in silicon carbide using femtosecond laser irradiation and acid etching *Appl. Surf. Sci.* **289** 529–32
[30] Li C, Shi X, Si J, Chen T, Chen F, Liang S, Wu Z and Hou X 2009 Alcohol-assisted photoetching of silicon carbide with a femtosecond laser *Opt. Commun.* **282** 78–80
[31] Iwatani N, Doan H D and Fushinobu K 2014 Optimization of near-infrared laser drilling of silicon carbide under water *Int. J. Heat Mass Transfer* **71** 515–20
[32] Stone H A, Stroock A D and Ajdari A 2004 Engineering flows in small devices: microfluidics toward a lab-on-a-chip *Annu. Rev. Fluid Mech.* **36** 381–411
[33] Liu G W, Muolo M L, Valenza F and Passerone A 2010 Survey on wetting of SiC by molten metals *Ceram. Int.* **36** 1177–88
[34] Naidich Y V, Zhuravlev V and Krasovskaya N 1998 The wettability of silicon carbide by Au–Si alloys *Mater. Sci. Eng.* **A245** 293–9
[35] Galli G, Catellani A and Gygi F 1999 Wetting silicon carbide with nitrogen: a theoretical study *Phys. Rev. Lett.* **83** 2006–9
[36] Kubiak K J, Wilson M C T, Mathia T G and Carval P 2011 Wettability versus roughness of engineering surfaces *Wear* **271** 523–8
[37] Akbari M, Sinton D and Bahrami M 2009 Pressure drop in rectangular microchannels as compared with theory based on arbitrary cross section *J. Fluids Eng.* **131** 041202
[38] Tsai C-H, Tai C-H, Fu L-M and Wu F-B 2004 Experimental and numerical analysis of the geometry effects of low-dispersion turns in microfluidic systems *J. Micromech. Microeng.* **15** 377–85
[39] Maselli V, Osellame R, Cerullo G, Ramponi R, Laporta P, Magagnin L and Cavallotti P L 2006 Fabrication of long microchannels with circular cross section using astigmatically shaped femtosecond laser pulses and chemical etching *Appl. Phys. Lett.* **88** 191107
[40] Weilin Q, Mala G M and Dongqing L 2000 Pressure-driven water flows in trapezoidal silicon microchannels *Int. J. Heat Mass Transfer* **43** 353–64
[41] Cheng Y, Sugioka K, Midorikawa K, Masuda M, Toyoda K, Kawachi M and Shihoyama K 2003 Control of the cross-sectional shape of a hollow microchannel embedded in photostructurable glass by use of a femtosecond laser *Opt. Lett.* **28** 55–7
[42] Dong Y and Molian P 2003 Femtosecond pulsed laser ablation of 3C–SiC thin film on silicon *Appl. Phys.* A **77** 839–46